In Situ X-Ray Diffraction Analysis of Microstructure Evolution during Deep Cryogenic Treatment and Tempering of Tool Steels

Chengsong Cui,* Juan Dong, Jérémy Epp, Alwin Schulz, Matthias Steinbacher, Serdal Acar, Sebastian Herbst, and Hans Jürgen Maier

Deep cryogenic treatment of tool steels, incorporated in conventional hardening and tempering, has been a topic of intensive research in recent years. Yet, the governing microstructural mechanisms involved in the deep cryogenic treatment of high-alloyed tool steels are still controversial. Thus, an in situ X-ray diffraction study is conducted on three tool steels X38CrMoV5-3, X153CrMoV12, and ~X190CrVMo20-4 to shed light on microstructural evolution during cryogenic treatment and subsequent tempering. For these high-alloyed tool steels, the transformation of retained austenite into martensite is detected during the cooling phase of the cryogenic treatment. A change in tetragonality of martensite occurs mainly in the heating phase of the subsequent tempering process, which indicates the diffusion of carbon and carbide precipitation from the martensite. The microstructure evolution of the tool steels after hardening, cryogenic treatment, and tempering is further examined by scanning electron microscopy.

1. Introduction

The effects of deep cryogenic treatment (DCT), incorporated in conventional heat treatment process with hardening and tempering, on the microstructure and mechanical properties of tool steels have been intensively studied over the last few decades.[1–3] It is reported by many researchers that DCT leads to improved mechanical properties such as high hardness, improved ductility, and fatigue properties as well as enhanced wear resistance.[4–7]

Dr. C. Cui, Dr. J. Dong, Dr. J. Epp, Dr. A. Schulz, Dr. M. Steinbacher
Leibniz-Institute for Materials Engineering – IWT
MAPEX Centre for Materials and Processes
University of Bremen
Badgasteiner Straße 3, 28359 Bremen, Germany
E-mail: cscui@iwt.uni-bremen.de

S. Acar, Dr. S. Herbst, Prof. H. J. Maier
Institut für Werkstoffkunde
Leibniz Universität Hannover
An der Universität 2, 30823 Garbsen, Germany

ⓘ The ORCID identification number(s) for the author(s) of this article can be found under https://doi.org/10.1002/srin.202100076.

These improvements in mechanical properties are attributed to an almost complete transformation of retained austenite into martensite and the formation of fine and homogeneously distributed special carbides in martensite.[2,3,8]

After conventional quenching to room temperature, retained austenite is present in high-alloyed tool steels. As a general practice, tool steels are tempered several times to convert the undesirable retained austenite into martensite and thus achieve dimensional stability and improved wear resistance. The austenite-to-martensite transformation can also take place upon further cooling of the quenched steels to cryogenic temperatures. For carburized or high-carbon steels, it is widely reported that there is almost complete transformation of the retained austenite at $-80\,^{\circ}$C (cold treatment) and further cooling to $-196\,^{\circ}$C (DCT) has no significant effect on the austenite-to-martensite transformation.[9,10] In contrast, it is reported that the formation of martensite in low-alloyed steels such as as-quenched AISI 52100 continues during all stages of DCT, i.e., cooling, isothermal holding, and reheating.[11]

Martensite in steels is a supersaturated solid solution of carbon in the interstitial sites of the initially body-centered cubic (bcc) iron, with a structure that is a distorted (tetragonal, bct) version of the equilibrium ferrite structure. The tetragonality of martensite increases linearly with the carbon concentration, in particular in the high carbon range above 0.6 mass%. Depending on the alloying elements, the c/a ratio will be between 1.08 and 1.00.[12] When the carbon content is below 0.2 mass%, the martensite structure should become bcc with a significantly increased dislocation density at room temperature.[13,14] However, it is questionable if the low tetragonality provoked by such small amount of carbon could have been detected experimentally in these earlier publications. During tempering, the diffusion of carbon from the martensite reduces the tetragonality of the martensite. Depending on the temperature of tempering, carbon atoms are then available for carbide precipitation.

It has been proposed that the formation of martensite at cryogenic temperature deforms the primarily formed martensite due to the volume effect of the martensitic transformation. In addition, the thermal expansion of martensite and austenite may cause additional plastic deformation in the vicinity of

ADVANCED
SCIENCE NEWS
www.advancedsciencenews.com

steel
research
international

www.steel-research.de

Frank's interfaces and increase local dislocation density. The resulting lattice strains force carbon atoms to diffuse to neighboring dislocations and defects, resulting in the formation of C-clusters and consequently promoting the formation of a large number of very fine carbides during subsequent tempering.[10,15–18]

Overall, the mechanisms of the structural changes that occur in a DCT are still not fully understood. As a consequence of this lack of understanding, the large scatter in data on the improvement of tool life of steel products reported in the literature remains largely unexplained and DCT is still not accepted widely in industrial practice.[19,20]

The present study was performed to shed light on the microstructure changes induced by DCT and the subsequent tempering. Specifically, laboratory X-ray diffractometers have been used to examine the phase transformation of three tool steels X38CrMoV5-3, X153CrMoV12, and ~X190CrVMo20-4 during cryogenic treatment and during subsequent tempering. This allowed to follow both the transformation of retained austenite into martensite and the change in tetragonality of martensite during the process. In addition, the microstructure evolution of the tool steels after hardening, cryogenic treatment, and tempering was also examined by scanning electron microscopy (SEM).

2. Experimental Section

2.1. Investigated Material

Three tool steels were analyzed in this article: the hot-working tool steel X38CrMoV5-3, the cold-working tool steel X153CrMoV12 (AISI D2), and the plastic mold steel ~X190CrVMo20-4. The X38CrMoV5-3 was manufactured by electro slag remelting and the other steels by powder metallurgy. The chemical composition of the tool steels was measured by optical emission spectrometry (S-OES, ARL3460), as listed in **Table 1**.

The samples for the in situ XRD analysis were taken from a block of X38CrMoV12 (cross section 106 mm × 206 mm), a rod of X153CrMoV12 (22 mm diameter), and a rod of ~X190CrVMo20-4 (21 mm diameter), respectively. The samples had a diameter of 20 mm and a thickness of 2 mm and their circular plan surfaces were ground prior to the XRD measurement.

The samples of X38CrMoV5-3 and X153CrMoV12 were austenitized in a two-chamber vacuum furnace (Ipsen RVTC) at 1050 °C for 30 min and quenched by 6 bar nitrogen gas to ≈60 °C, followed by cooling to room temperature in ambient air. The samples of ~X190CrVMo20-4 were austenitized at 1150 °C for 30 min and quenched in the same way. Some of the samples

Table 1. Chemical composition of the tool steels measured by spark optical emission spectrometry (mass%).

Alloy	C	Si	Mn	Cr	Mo	V	W
X38CrMoV5-3	0.39	0.35	0.35	4.93	2.87	0.50	0.08
X153CrMoV12	1.52	0.28	0.27	11.38	0.87	0.85	0.02
~X190CrVMo20-4[a]	1.99	0.62	0.29	19.7	1.02	4.02	0.46

[a]The steel ~X190CrVMo20-4 is not standardized, and is therefore designated with the tilde.

were characterized by in situ XRD measurement directly after quenching (for phase analysis during DCT). The other samples were further cryogenically treated in liquid nitrogen at boiling temperature for 40 h, and then used for in situ XRD analyses during subsequent tempering. For the in situ XRD analysis, the samples were electrochemically etched to remove a surface layer of ≈50 μm with acidic electrolyte. To avoid possible stabilization of retained austenite, the XRD measurements were started within 2 h after quenching/cryogenic treatment.

The microstructural evolution was also characterized by SEM after different heat treatments, i.e., quenching (Q), quenching + DCT (Q + C), and quenching + DCT + single tempering (Q + C + T$_1$). For the SEM study, rectangular samples (1 mm × 10 mm × 10 mm) were used. The DCT of these samples was also performed in liquid nitrogen for 40 h. The tempering temperature was 560, 530, and 525 °C for X38CrMoV5-3, X153CrMoV12, and ~X190CrVMo20-4, respectively. The samples were ground and mechanically and electrolytically polished. Detailed information about the heat treatment parameters is given in the study by Schulz et al.[21] and the electrolytic polishing parameters can be found in the study by Acar et al.[22]

2.2. In Situ XRD Analysis

2.2.1. Deep Cryogenic Treatment

The setup used for the in situ XRD measurement during DCT is shown in **Figure 1**a. The DCT of a sample for the measurement is shown in Figure 1b. The sample was mounted at the top of an aluminum rod, which was cooled by liquid nitrogen filled inside a thermally isolated container. A thermocouple (type K, class 3, 0.5 mm diameter) was inserted in a hole (0.6 mm diameter, 5 mm depth) located in the center of the sample (2 mm thickness) parallel to the surface for measuring the temperature during the experiments. In this investigation, the samples were cooled from ambient temperature to nearly the boiling temperature of liquid nitrogen, held for 15–30 min (since the main transformation processes were already completed here), and then reheated to ambient temperature in air. The cooling rate of the samples was 10–20 K min^{-1}. An X-ray diffractometer (ETA 3003, Seifert) equipped with a $\theta/2\theta$ goniometer and Cr Kα radiation (0.228975 nm) was used for the analyses with a primary beam diameter of 2 mm. The penetration depth of Cr Kα in steel was between 3 and 5 μm for the considered configuration. Full diffraction patterns were measured with a position-sensitive detector (PSD). For fast measurements, a 2θ range of 58° to 85° was covered and 58° to 113° was used for slower measurements that provided higher resolution. The acquisition time for one pattern was 90 s for the fast measurements (to measure in a small temperature range during cooling) and 600 s for the slow measurements (increased counting statistics). The heating of the samples to room temperature occurred naturally by removing the samples from the cooling device. The heating rate of the samples after the cryogenic treatment was 5 K min^{-1}.

2.2.2. Tempering

The setup used for the in situ XRD experiments during tempering is shown in **Figure 2**. A sample was mounted inside a furnace
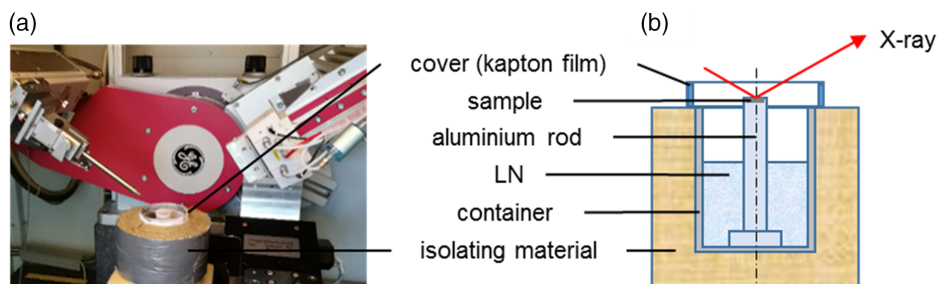
Figure 1. a) Setup of the in situ XRD analyses during DCT and b) illustration of the DCT for in situ XRD experiments.

heated by an electrical resistance heating element. A heating element was applied to the back-face of the sample whereas the front side of the sample was analyzed. During the slow heating, there were no pronounced temperature gradients within the sample. The furnace was continuously purged with nitrogen gas to prevent oxidation and decarburization of the sample. A thermocouple (type K, class 1, 0.5 mm diameter) was inserted in the outer circumference of the samples for the temperature control. In this investigation, the deep cryogenically treated samples were heated to 560, 530, and 525 °C for X38CrMoV5-3, X153CrMoV12, and ~X190CrVMo20-4, respectively. The heating rate was $10\,K\,min^{-1}$. After holding at tempering temperature for 1 h, the samples were cooled in nitrogen gas at a rate of $50\,K\,min^{-1}$. The XRD measurements were performed before, during, and after the tempering process. A diffractometer (D8, Bruker-AXS) equipped with a $\theta/2\theta$ goniometer, a rotating anode, and a fast PSD using Co Kα radiation (0.178889 nm) was used for the analyses with a primary beam diameter of about 3 mm. The penetration depth of Co Kα reached up to 11 µm in the configuration used. Complete diffraction patterns were recorded over a 2θ range of 43° to 103° with a step size of 0.1°. The measurements during the heating phase took ≈150 s each, i.e., each of these measurements was performed within a temperature range of 25 °C. Before heating and after cooling to ambient temperature, the samples were precisely measured over a 2θ range of 42° to 130° in ≈30 min, leading to high-quality diffraction patterns.

For diffraction patterns analysis, the Rietveld method provided within the software Topas 4.2 (Bruker-AXS) was used. The quantitative analysis of the phases was focused on martensite and austenite, whereas the quantity of carbides was also determined by fitting using the software Topas. Previous XRD measurements of the three steels have already shown that the carbides, especially in the steels X153CrMoV12 and ~X190CrVMo20-4, could hardly be detected precisely. The fine dispersed different carbides gave rise to diffraction peaks with very low intensity, peak overlap, and overlap with the peaks of martensite and austenite, and therefore, these cannot be detected precisely in fast in situ measurements. Therefore, only the total amount of carbide was presented in the results without giving the single content of each carbide type. The carbide types taken into account were as follows: M_3C, M_7C_3, and $M_{23}C_6$.

2.3. Scanning Electron Microscopy

The microstructural evolution during the heat treatment was also characterized by electron microscopy. For SEM work, a ZEISS Supra 55 VP SEM was used and images were recorded at a nominal acceleration voltage of 15 kV.

3. Results and Discussion

3.1. XRD Analysis of Microstructure Evolution during DCT

The XRD patterns of the tool steels before, during, and after the DCT are shown in **Figure 3**. The main peaks of martensite and austenite are marked in the diagrams.

The XRD patterns of the X38CrMoV5-3 sample at different stages of the DCT appear very similar. It is hard to identify the peaks of austenite from the XRD patterns. The austenite content was determined to be ≈3 mass%, which is within the intrinsic uncertainty of the method (at least ±3 mass%).

The main differences in the XRD patterns of the X153CrMoV12 sample at different stages of the DCT are the austenite peaks. The as-quenched sample shows higher intensity of the austenite peaks. The austenite peak intensity decreases during cooling of the sample. Reheating to ambient temperature (after cryogenic treatment) does not cause remarkable changes of the austenite peaks. The martensite peaks are not visibly affected by the DCT.

For ~X190CrVMo20-4, the austenite peaks in the XRD pattern of the as-quenched sample show high intensity. They are strongly reduced at deep cryogenic temperature. After reheating to room temperature (after cryogenic treatment), no further change was observed.
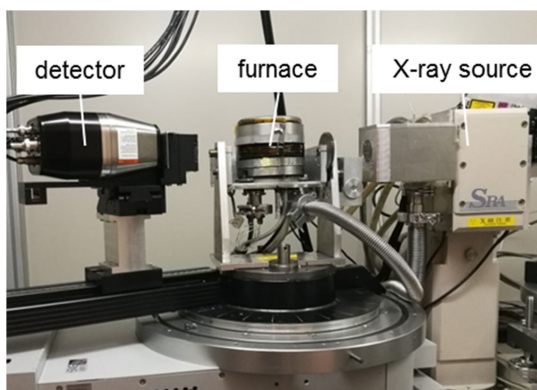

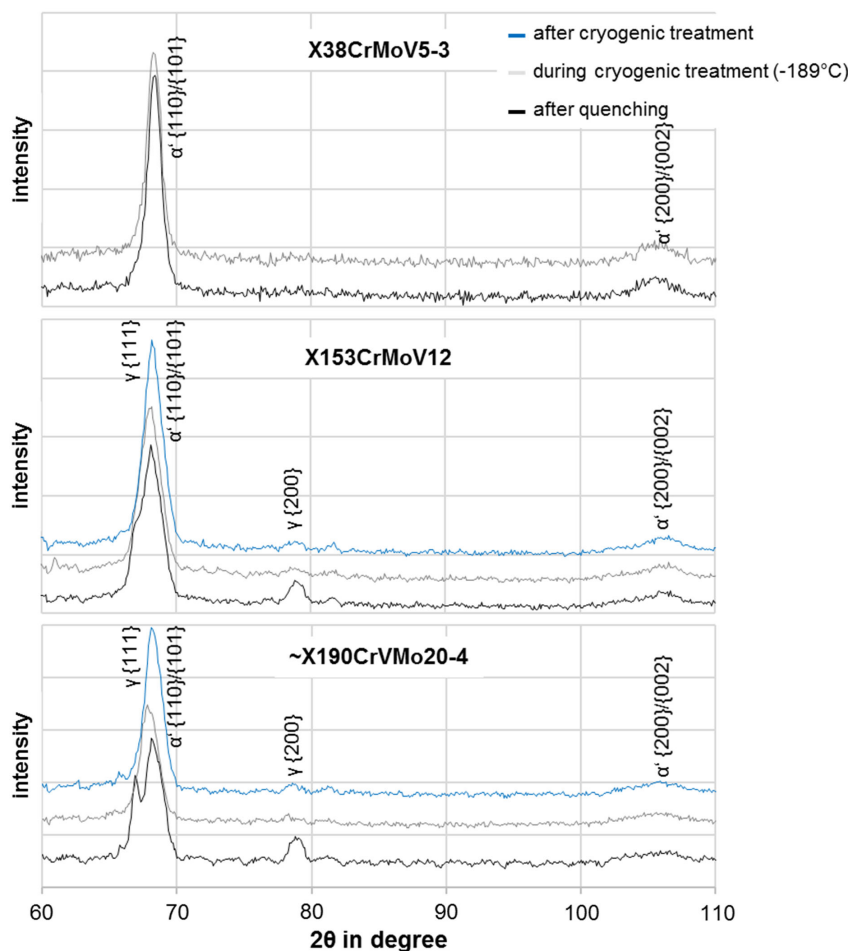**Figure 2.** Setup used for in situ XRD measurement during tempering.

Figure 3. XRD patterns (Cr Kα radiation) of the tool steels X38CrMoV5-3, X153CrMoV12, and ~X190CrVMo20-4 recorded during DCT.

The martensite peaks in the XRD patterns remain almost unchanged during the DCT for all the investigated tool steels. The tetragonality of the martensite, defined as the c/a ratio of the lattice parameters c and a, which is related to the carbon content in the martensite, has been examined. No significant change in the tetragonality of martensite during the DCT was observed. For example, the c/a ratio of the martensite in the ~X190CrVMo20-4 is about 1.022 at different stages of the DCT. This result is consistent with the observations of the tetragonality of martensite in 100Cr6 during subzero cooling to 133 K in the study by Villa et al.[11] This suggests that no carbon diffusion from the martensite and carbide precipitation occurs during the DCT, which is in contrast to the observations by Tyshchenko et al.[18] The later reported an abnormally low tetragonality of the virgin martensite formed at low temperatures, and attributed this effect to the capture of carbon atoms by moving dislocations. Consequently, the carbon content in the martensitic solid solution, and thus tetragonality are decreased.

In addition, it is difficult to detect and identify carbides due to short measurement times and low peak intensities or low signal-to-noise ratio. The use of a diffractometer with 2D detector or using synchrotron radiation facilities could help to detect the carbides properly.

The austenite-to-martensite transformation in the tool steels X153CrMoV12 and ~X190CrVMo20-4 during the cryogenic treatment, evaluated quantitatively by Rietveld refinements, is shown in **Figure 4** and **5**.

The retained austenite content of the X153CrMoV12 steel decreases particularly in the temperature range from 10 °C to −40 °C. During continued cooling to −186 °C, no further reduction of austenite was detected. The content of the remaining retained austenite is ≈3–5 mass%. When the sample is reheated to ambient temperature, the austenite is not transformed as well. The transformation of the retained austenite in the ~X190CrVMo20-4 steel is similar to that in the X153CrMoV12 but the phase transformation takes place over a wider temperature range from RT to −80 °C.

Due to a very low level of retained austenite in the X38CrMoV5-3 in the as-quenched state, a change in the content of the retained austenite during the DCT could not be detected.

3.2. XRD Analysis of Microstructure Evolution during Tempering

The XRD patterns of the deep cryogenically treated tool steels before and after tempering are shown in **Figure 6**. The main
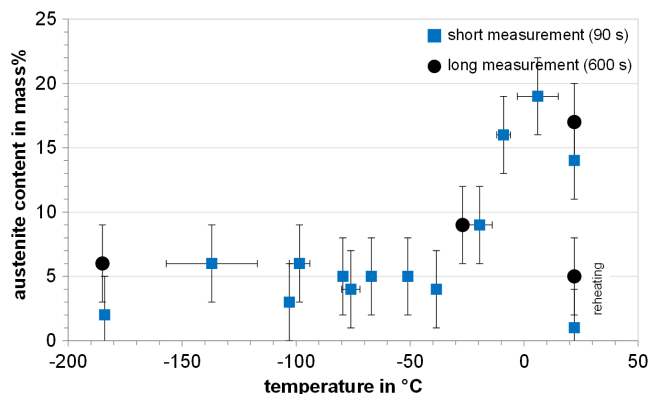
Figure 4. Evolution of retained austenite content during DCT of X153CrMoV12. The temperature ranges in which the measurements were made are also plotted in the diagrams (horizontal bar).
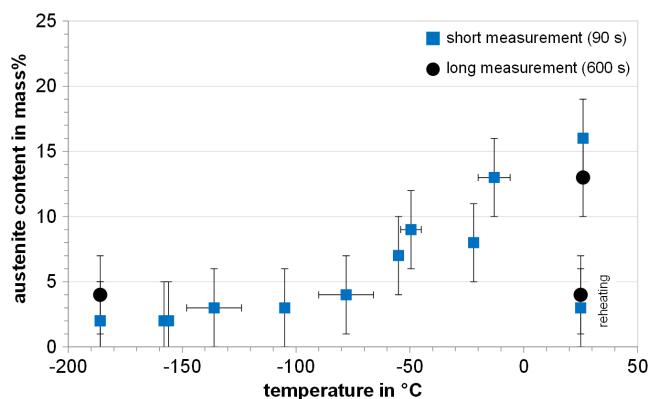

Figure 5. Evolution of retained austenite content during DCT of ~X190CrVMo20-4. The temperature ranges in which the measurements were made are also plotted in the diagrams (horizontal bar).

Figure 6. XRD patterns (Co Kα radiation) of the deep cryogenically treated tool steels X38CrMoV5-3, X153CrMoV12, and ~X190CrVMo20-4 before and after tempering.

peaks of martensite and austenite are marked in the diagrams. The most significant difference between the patterns is the peak width of the martensite peaks, particularly for the steels X153CrMoV12 and ~X190CrVMo20-4. The peak width evolution of the martensite suggests that the tetragonality of martensite changed during tempering. The tetragonality of martensite, which is caused by the carbon atoms remaining in the octahedral sites along the c axis of the lattice during the transformation of austenite to martensite, contributes to higher full width at half maximum (FWHM) values. The tetragonality of martensite is also known to increase linearly as carbon content increases.[23] In contrast, the reduction of dislocation density and lattice strains during tempering also influences the peak broadening and both effects can be taken into account by using the Rietveld method.

Details of the changes in the phases and the tetragonality of martensite in the heating phase as well as in the holding phase of the tempering of the deep cryogenically treated tool steels are shown in **Figure 7–9**.

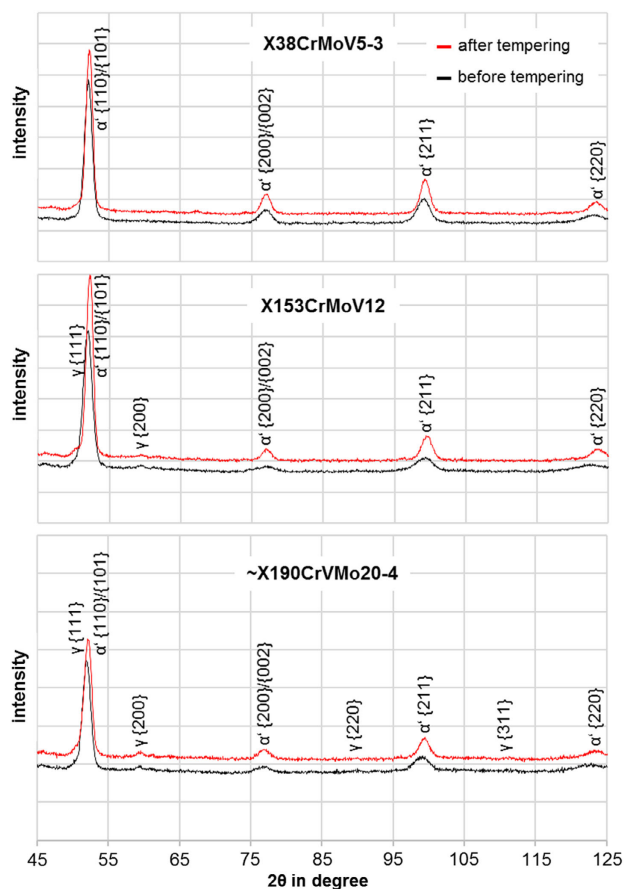For the X38CrMoV5-3 steel, the content of martensite is nearly constant during tempering, whereas the amount of retained austenite decreases slightly and the content of carbides (M_3C) increases slightly, especially during holding at 560 °C for 1 h. The tetragonality ratio c/a decreases slightly during the heating phase. The martensite was found to have relative low tetragonality as expected for the steel with about 0.38 mass% carbon. Based on previous studies, it is expected that the martensitic lattice loses its tetragonality during tempering and the carbon atoms that are trapped in the "c" octahedral sites of the supersaturated martensite by quenching or DCT diffuse out to precipitate as carbides during tempering.[24]

For the X153CrMoV12 steel, the contents of the main phases such as martensite, austenite, and carbides (M_3C, $M_{23}C_6$, and M_7C_3) are almost unchanged in the heating phase and in the holding phase. However, the lattice parameters c and a change remarkably in the heating phase, i.e., with increasing temperature the parameter c decreases, whereas the parameter a increases. Consequently, the tetragonality ratio c/a decreases continuously. This indicates carbon depletion from the martensite and precipitation as carbides in the heating phase of the tempering, particularly between 150 and 200 °C. This effect is consistent with the theory on tempering of martensite.[25] The lattice parameters hardly change in the holding phase (1 h at 530 °C) of the tempering.
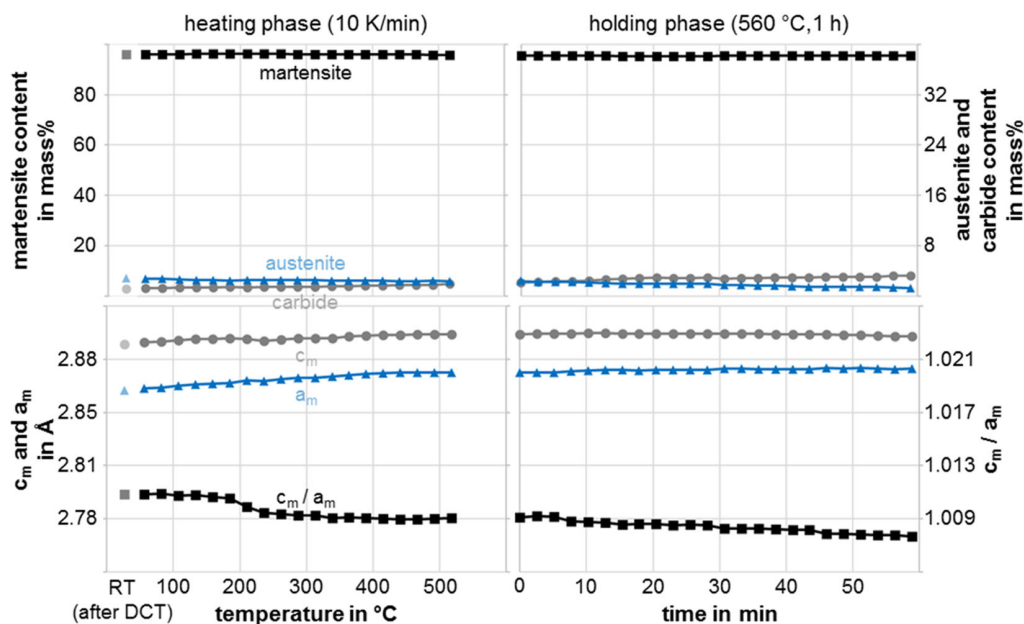
ADVANCED
SCIENCE NEWS
www.advancedsciencenews.com

steel
research
international

www.steel-research.de

Figure 7. Evolution of microstructure constituents and lattice parameters of the deep cryogenically treated tool steel X38CrMoV5-3 during subsequent tempering.
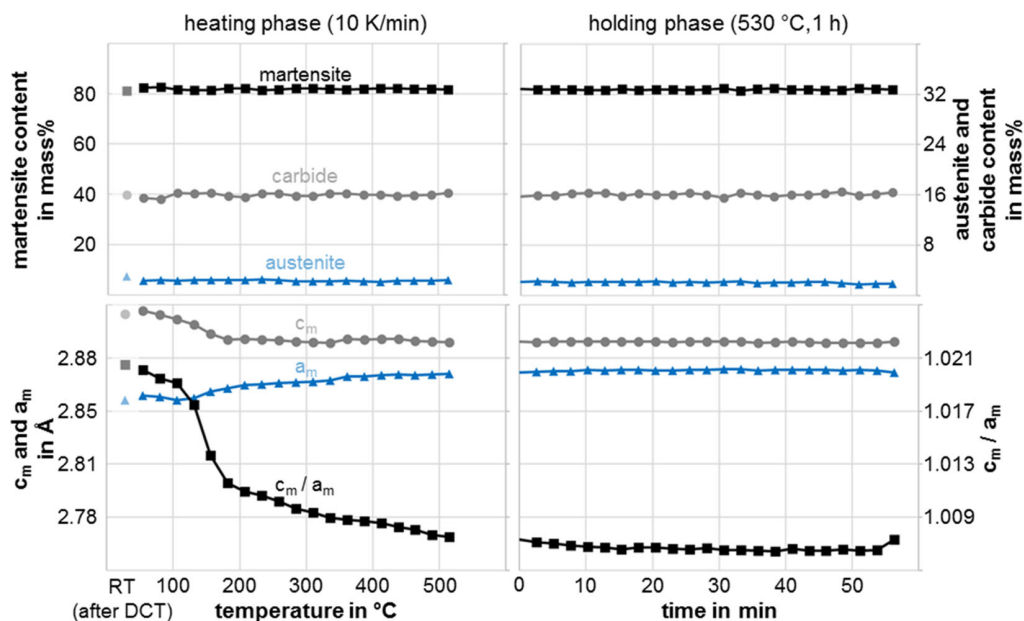

Figure 8. Evolution of microstructure constituents and lattice parameters of the deep cryogenically treated tool steel X153CrMoV12 during subsequent tempering.

For the ~X190CrVMo20-4 steel, the contents of the martensite, retained austenite, and the carbides (M_3C, $M_{23}C_6$, and M_7C_3) do not show significant change during heating and holding for 1 h at 525 °C. The lattice parameter c/a decreases mainly in the heating phase, but less pronounced than in the X153CrMoV12 steel, also suggesting depletion of carbon from the martensite and carbide precipitation.

It is difficult to precisely identify the carbides in the XRD patterns of the tool steels due to the low signal-to-noise ratio of the new precipitated very fine carbides. Therefore, the changes in the carbide contents are not obvious although the loss of tetragonality of martensite is observed during the tempering, i.e., the precipitated carbides are too small for detection under the experimental condition but can be deduced indirectly from the decreased c/a ratio. Based on the following model between c/a and carbon content $C\%$ of martensite,[26] the depletion of carbon in martensite after tempering is estimated to be ≈0.10% for X38CrMoV5-3, 0.32% for X153CrMoV12, and 0.11% for
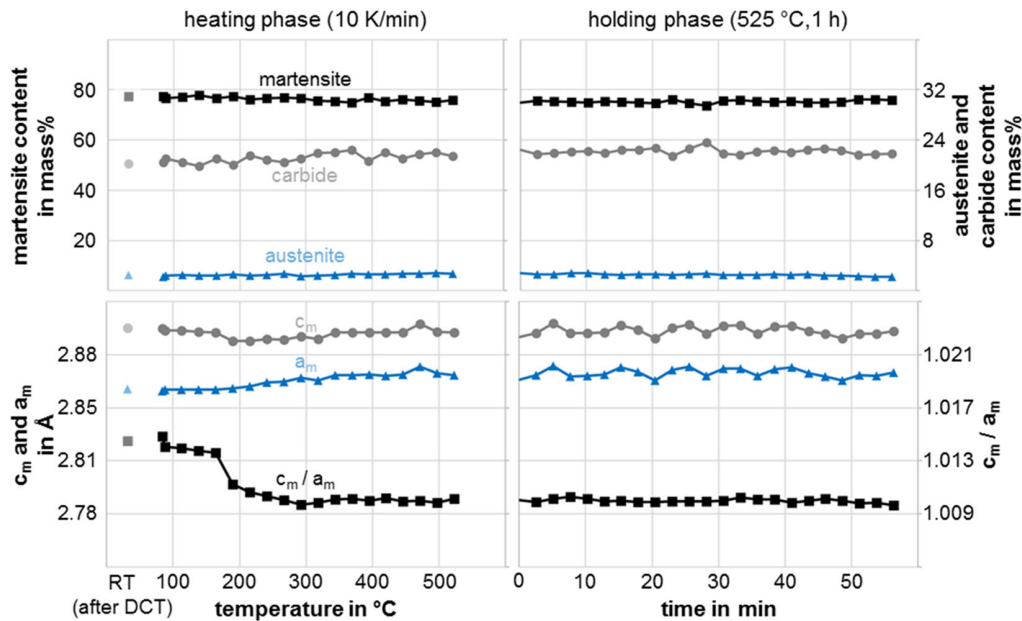
Figure 9. Evolution of microstructure constituents and lattice parameters of the deep cryogenically treated tool steel ~X190CrVMo20-4 during subsequent tempering.

~X190CrVMo20-4. It indicates that the amount of carbides which is expected to precipitate during tempering is rather small, particularly for X38CrMoV5-3 and ~X190CrVMo20-4 (1–2% carbide precipitates).

$$C\% = \left(\frac{\frac{c}{a} - 1}{0.0443} \right) \qquad (1)$$

3.3. Microstructure under Different Heat Treatment Conditions

The SEM images of the tool steels X38CrMoV5-3, X153CrMoV12, and ~X190CrVMo20-4 in different heat treatment conditions (quenching (Q), quenching + DCT (Q + C), and quenching + DCT + single tempering (Q + C + T₁)) are shown in **Figure 10**.

After quenching (Q), the microstructure of X38CrMoV5-3 consists of hardened martensite with primary carbides, which did not dissolve during austenitization. The carbides have a spherical shape with a diameter of smaller than 1 μm. As shown in Sections 3.1 and 3.2, the volume fraction of retained austenite is very low and cannot be clearly detected here. Lath martensite is present in a spear-pointed form, which can also be found in the Q + C state. As already seen in the XRD results, there is practically no influence of cryogenic treatment on the microstructure of X38CrMoV5-3. The martensite consists of parallel latticed laths, which are grouped in packages. After hardening, carbon atoms can be enriched along lath interfaces and at dislocations inside the laths. Tempering changes the thermodynamically unstable martensitic structure into a state that is closer to equilibrium. A complete tempering process of steels include normally 1) segregation of carbon, 2) precipitation of carbides, and 3) recovery and recrystallization of the microstructure.

For the tool steels in the current heat treatment condition, the first two changes could occur, whereas the recovery and recrystallization should hardly happen for retaining enough hardness and strength. Through tempering, dislocations are first removed which triggers the building of precipitations.[27] Figure 10 shows that tempering (Q + C + T₁) of X38CrMoV5-3 leads to the precipitation of carbides, especially at the lath interfaces. The interfaces and dislocations within the laths act as nucleation sites for precipitation during tempering.[28] However, a chemical composition of these carbides could not be determined by energy dispersive X-ray spectroscopy (EDS). Given the small size of the carbides, the interaction volume is significant and large contributions from the matrix would affect the EDS signal. In this context, a focused ion beam (FIB) lamella could provide information as to whether the carbides are cementite or alloyed carbides, transmission electron microscope investigations could be used to determine the carbide type.

After quenching (Q), the steel X153CrMoV12 consists of a martensitic structure of plate martensite with embedded carbides. The ledeburitic steel X153CrMoV12 contains a high amount of carbon and alloying elements Cr, Mo, and V, which form carbides. Compared to X38CrMoV5-3, the steel X153CrMoV12 has a higher number of primary carbides, which in addition are larger in diameter. The carbides that remain undissolved during austenitization have great influence on the wear resistance of tool steels. As the XRD patterns have already shown, there is still retained austenite after hardening (Q), which is transformed into virgin martensite by the cryogenic treatment (Q + C). The virgin martensite has a fine twin structure, a lower tetragonality, a lower strength, and a relatively high ductility compared to as-quenched martensite.[29] In summary, the martensite crystals formed during Q + C are finer than the martensite formed during quenching.
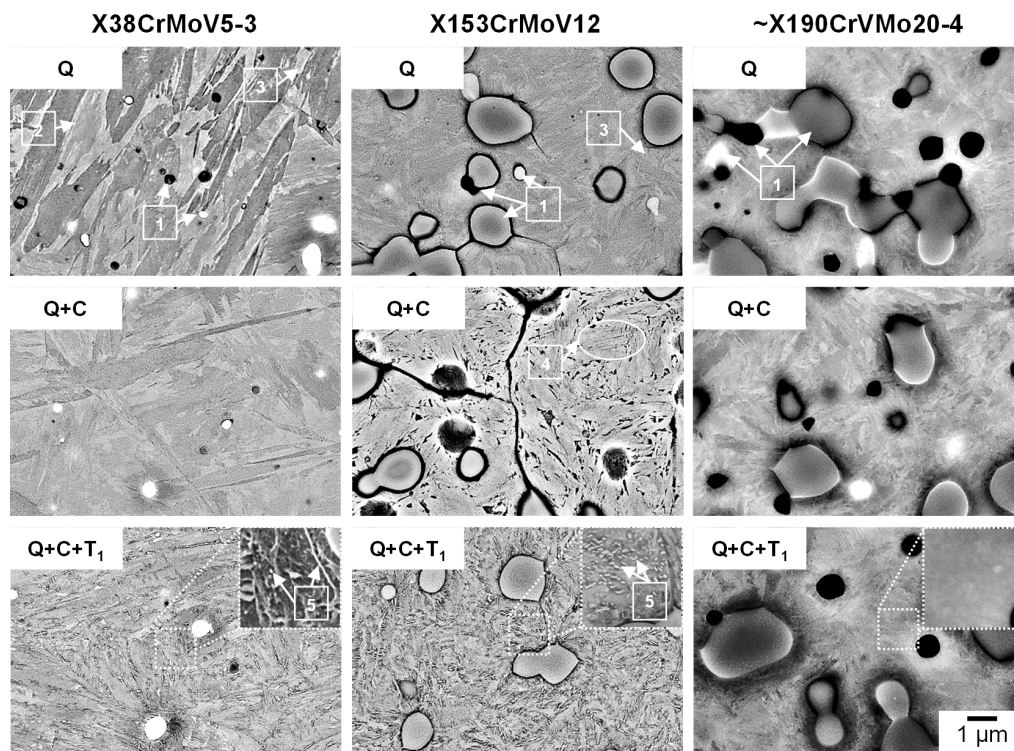
Figure 10. SEM images of the tool steels X38CrMoV5-3, X153CrMoV12, and ~X190CrVMo20-4 in different heat treatment conditions; 1-primary carbides, 2-martensite, 3-retained austenite, 4-martensite, and 5-secondary carbides.

A single tempering leads to the formation of carbides that are homogeneously distributed. During cryogenic treatment, a further transformation of retained austenite into martensite leads to a higher density of dislocations. The dislocations formed during martensitic transformation can move through the matrix due to progressive deformation, picking up C atoms from carbides due to their higher bonding enthalpy. In a subsequent tempering step, the clusters of carbon atoms pinned by dislocations act as nucleation points for the precipitation of nanocarbides. However, those carbides could not be detected in XRD measurements (Figure 8) due to their much smaller size and low content compared to the primary carbides.

The influence of a cryogenic treatment on the plastic mold steel ~X190CrVMo20-4 regarding austenite transformation is significant. After Q and Q + C, the SEM images show a martensitic structure with embedded carbides and retained austenite, with a lower austenite content and a finer martensite structure for Q + C. An increase in volume due to the martensitic transformation leads to compressive stresses in the retained austenite, which acts stabilizing and prevents further transformation. The volume fraction of primary carbides is the highest for ~X190CrVMo20-4 due to the high content of carbide forming elements. However, it is noted that after tempering (Q + C + T_1), there is no significant formation of secondary carbides as is the case of X38CrMoV5-3 and X153CrMoV12. This could be attributed to the strong binding energy of carbon in alloyed martensite and in complex carbides of the highly alloyed steel. The smaller reduction of c/a ratio and thus smaller reduction of carbon content of the ~X190CrVMo20-4 during tempering confirms this

result. For a carbide to precipitate, diffusion of carbon and the alloying elements is necessary. At low tempering temperatures up to about 450 °C, the carbon can diffuse, but not the alloying elements. Therefore, only iron carbide (cementite) can form when tempering alloyed steels at low temperatures. If higher tempering temperatures above 500 °C are applied, the mobility of the carbide-forming alloying atoms becomes high enough to form special carbides.

4. Conclusion

1) The transformation of residual austenite in the tool steels was observed and analyzed quantitatively via in situ XRD analysis performed during the DCT. Changes in the tetragonality of martensite and carbide precipitation could not be identified during the DCT process. Due to the very low initial content of retained austenite in the X38CrMoV5-3 in the as-quenched state, an austenite-to-martensite transformation during the DCT was not detected. For the X153CrMoV12 steel, the retained austenite content decreases particularly in the temperature range from 10 to −40 °C. No further residual austenite transformation could be observed during the DCT, which means that a small amount of austenite remained after the DCT. For the ~X190CrVMo20-4 steel, the transformation of the retained austenite mainly takes place in the temperature range from RT to −80 °C. 2) The in situ XRD investigations conducted during the tempering process of the hardened and deep cryogenically treated tool steels show that the martensite loses partially its tetragonality. However, it is not

possible to identify directly the precipitation of carbides in the XRD patterns which is due to the low signal of the low amount of additional carbides formed during tempering on the one hand and to the experimental conditions (short measuring time and complex microstructure) on the other hand. The tetragonality of martensite of the tool steels decreases during the heating mainly in the temperature range between 150 and 200 °C, which indicates carbon depletion in the martensite and thus carbide precipitation from the martensite. 3) The SEM examinations confirm the XRD results concerning the transformation of austenite into martensite during deep cryogenic cooling. The influence of cryogenic treatment on the precipitation behavior of carbides after single tempering is less pronounced in the tool steel ~X190CrVMo20-4 with a high proportion of carbide-forming alloying elements. This effect is attributed to higher binding energy of carbon in alloyed martensite and in complex carbides.

Conflict of Interest

The authors declare no conflict of interest.

Data Availability Statement

Data available on request from the authors.

[1] R. F. Barron, *Cryogenics* **1982**, *409–413*, 22.
[2] D. N. Collins, *Heat Treat. Met.* **1996**, *2*, 40.
[3] D. Das, A. K. Dutta, V. Toppo, K. K. Ray, *Mater. Manuf. Process.* **2007**, *22*, 474.
[4] A. Akhbarizadeh, A. Shafyei, M. A. Golozar, *Mater. Design* **2009**, *30*, 3259.
[5] D. N. Collins, J. Dormer, *Heat Treat. Met.* **1997**, *3*, 71.
[6] D. N. Collins, G. O'Rourke, in *Proc. of the 18th Conf. on Heat Treating* (Eds.: H. W. Walton, R. A. Wallis), ASM International, Materials Park, OH **1998**, p. 229.
[7] A. Oppenkowski, S. Weber, W. Theisen, *J. Mater. Process. Tech.* **2010**, *210*, 1949.
[8] K. Amini, A. Akhbarizadeh, S. Javadpour, *Mater. Des.* **2013**, *45*, 316.
[9] F. Dobler, T. Hoja, *Einfluss von tiefen Temperaturen auf die Festigkeitseigenschaften einsatzgehärteter und verzahnter Bauteile*, Abschlussbericht, IGF 16354N, **2013**.
[10] M. Villa, M. A. J. Somers, presented at *24th IFHTSE Congress 2017, European Conf. on Heat Treatment and Surface Engineering*, Nice, France, June 2017.
[11] M. Villa, K. Pantleon, M. A. J. Somers, *Acta Mater.* **2014**, *65*, 383.
[12] R. E. Smallman, A. H. W. Ngan, *Modern Physical Metallurgy*, 8th ed., Elsevier Ltd., Amsterdam **2014**.
[13] P. G. Winchell, M. Cohen, *ASM Trans. Quart.* **1962**, *55*, 347.
[14] X. Liu, F. Zhong, J. Zhang, M. Zhang, M. Kang, Z. Guo, *Phys. Rev. B* **1995**, *52*, 9970.
[15] D. Das, A. K. Dutta, K. K. Ray, *Wear* **2009**, *267*, 1371.
[16] F. Meng, K. Tagashira, R. Azuma, H. Sohma, *ISIJ Int.* **1994**, *34*, 205.
[17] P. F. Stratton, *Mater. Sci. Eng. A* **2007**, *449–451*, 809.
[18] A. I. Tyshchenko, W. Theisen, A. Oppenkowski, S. Siebert, O. N. Razumov, A. P. Skoblik, V. A. Sirosh, Y. N. Petrov, V. G. Gavriljuk, *Mater. Sci. Eng. A* **2010**, *527*, 7027.
[19] D. Das, A. K. Dutta, K. K. Ray, *Mater. Sci. Eng. A* **2010**, *527*, 2194.
[20] M. Pellizzari, D. Caliskanoglu, A. Fernandez, J. 1. Barbero, B. Pena, T. Uemit, R. Pizarro Sanz, R. Elvira Eguizabal, L. A. Alava, *HTM J. Heat Treatm. Mater.* **2012**, *67*, 111.
[21] A. Schulz, C. Cui, M. Steinbacher, T. Ümit, M. Wunde, I. Jung, S. Acar, F. Nürnberger, G. Gerstein, S. Herbst, H. J. Maier, *HTM J. Heat Treatm. Mat.* **2020**, *75*, 287.
[22] S. Acar, G. Gerstein, C. Cui, A. Schulz, F. Nürnberger, *Pract. Metallogr.* **2019**, *56*, 303.
[23] M. Narazaki, G. E. Totten, G. M. Webster, in *Handbook of Residual Stress and Deformation of Steel* (Eds. G. E. Totten, M. Howes, T. Inoue), ASM International, Materials Park, OH **2002**, p. 248.
[24] N. Xu, G. P. Cavallaro, A. R. Gerson, *Mater. Sci. Eng. A* **2010**, *527*, 6822.
[25] A. Stojko, PhD Thesis, The Technical University of Denmark (DTU), Kgs. Lyngby, Denmark **2006**.
[26] L. Cheng, A. Böttger, Th. H. de Keijser, E. J. Mittemeijer, *Scr. Metall. Mater.* **1990**, *24*, 509.
[27] G. R. Speich, W. C. Leslie, *Metall. Trans.* **1972**, *3*, 1043.
[28] T. Furuhara, K. Kobayashi, T. Maki, *ISIJ Int.* **2004**, *44*, 1937.
[29] G. T. Eldis, M. Cohen, *Metall. Trans. A* **1983**, *14*, 1007.